INL/JOU-23-72391-Revision-0

Analysis of radially resolved thermal conductivity in high burnup mixed oxide fuel and comparison to thermal conductivity correlations implemented in fuel performance codes

Joshua Ferrigno, Tsvetoslav R Pavlov, Narayan Poudel, Daniele Salvato, Chuting Tan Tsai, Brian Merritt, Alex Hansen, Troy Munro, Fabiola Cappia, Marat Khafizov

Changing the World's Energy Future

Idaho National Laboratory

INL is a U.S. Department of Energy National Laboratory operated by Battelle Energy Alliance, LLC

DISCLAIMER

This information was prepared as an account of work sponsored by an agency of the U.S. Government. Neither the U.S. Government nor any agency thereof, nor any of their employees, makes any warranty, expressed or implied, or assumes any legal liability or responsibility for the accuracy, completeness, or usefulness, of any information, apparatus, product, or process disclosed, or represents that its use would not infringe privately owned rights. References herein to any specific commercial product, process, or service by trade name, trade mark, manufacturer, or otherwise, does not necessarily constitute or imply its endorsement, recommendation, or favoring by the U.S. Government or any agency thereof. The views and opinions of authors expressed herein do not necessarily state or reflect those of the U.S. Government or any agency thereof.

INL/JOU-23-72391-Revision-0

Analysis of radially resolved thermal conductivity in high burnup mixed oxide fuel and comparison to thermal conductivity correlations implemented in fuel performance codes

Joshua Ferrigno, Tsvetoslav R Pavlov, Narayan Poudel, Daniele Salvato, Chuting Tan Tsai, Brian Merritt, Alex Hansen, Troy Munro, Fabiola Cappia, Marat Khafizov

August 2024

Idaho National Laboratory
Idaho Falls, Idaho 83415

http://www.inl.gov

Prepared for the
U.S. Department of Energy
Under DOE Idaho Operations Office
Contract DE-AC07-05ID14517, DE-AC07-05ID14517

Analysis of radially resolved thermal conductivity in high burnup mixed oxide fuel and comparison to thermal conductivity correlations implemented in fuel performance codes

Joshua Ferrigno[a], Tsvetoslav Pavlov[b], Narayan Poudel[b], Daniele Salvato[b], Chuting Tsai[b], Brian Merritt[c], Alex Hansen[c], Troy Munro[c], Fabiola Cappia[b], Marat Khafizov[a]

[a]The Ohio State University, Dept. of Mechanical and Aerospace Engineering

[b]Idaho National Laboratory

[c]Brigham Young University, Dept. of Mechanical Engineering

Abstract

The thermal diffusivity and thermal conductivity of high burnup (19% FIMA) mixed oxide (U, Pu)O_2 nuclear fuel has been measured along the radial direction using a thermoreflectance-based method. Measured thermal conductivity exhibits a notable radial variation consistent with the expectations that a large temperature gradient across the annular fuel pellet leads to a heterogeneous microstructure. A common fuel performance model of thermal conductivity, the Lucuta-Inoue model, is used to analyze the measured thermal conductivity profile. This model adequately captures the radial dependence of thermal conductivity except in the periphery. The analysis suggests that the characteristic radial shape of the thermal conductivity profile follows the burnup profile within the fuel pin. In the periphery, the high burnup structure is formed and the conductivity model, not capturing this effect, likely overestimates the thermal conductivity.

Keywords: thermal conductivity, thermoreflectance, nuclear energy, mixed-oxide fuel

1. Introduction

As burnup increases over the life of nuclear fuel, it exhibits drastic microstructural, compositional, and physical property changes due to the conditions of its extreme environment (*1*). Neutron irradiation introduces point defects, dislocation loops, stoichiometric changes, fission product dispersal, and porosity (*2, 3*). The extent to which defects are present in the fuel greatly affects its thermophysical properties. The extreme temperature gradients across the fuel pin lead to local spatial variations in the microstructure, defect population, and physical properties of the fuel (*4, 5*). As reactor developers, regulators, and utilities all seek to improve thermal efficiency and safety, many have placed a large effort on the development of advanced fuel performance codes (FPC) (*6-9*). These serve to simulate and predict the thermo-mechanical behavior of nuclear fuels under reactor conditions and thereby optimize plant operations. In particular, thermal conductivity determines the temperature profile across the fuel pin at steady conditions while also being of significant importance for modeling non-instantaneous transient conditions. Currently, nuclear fuel performance models are based on the parametrization of post-irradiation examination (PIE) of nuclear fuels that have been irradiated under a variety of normal and off-normal conditions (*4, 6, 10*). Oftentimes, self-irradiation of nuclear fuel occurs during storage which can complicate the as irradiated and PIE measurement comparisons (*1, 11*).

This work focuses on understanding the thermal conductivity (k) in irradiated nuclear fuels. In contrast to previous reports utilizing laser flash apparatus to measure these properties (*12-14*), the current study provides a unique ability to quantify thermal transport properties with microscale resolution across the radial profile of a fuel pellet. This work utilizes a thermal conductivity microscope (TCM) to experimentally measure thermal conductivity with micron resolution (*15*). While the TCM provides a reliable measurement of thermal diffusivity, thermal conductivity can be determined in certain conditions as well (*16*). There have been several studies assessing the ability to use the TCM to investigate the impact of ion-irradiated induced defects on the thermal conductivity of fuel surrogates (*17-22*), yet fewer have been conducted on neutron-irradiated nuclear fuels. Local measurements of the thermal conductivity profile of neutron-irradiated nuclear fuels have recently been demonstrated (*23, 24*).

The focus of this work is a mixed oxide (MOX) fuel irradiated under prototypical fast neutron reactor conditions. Sodium Fast Reactor (SFR) oxide fuels experience significant radial temperature gradients (>1000°C change in temperature between center and periphery). Thus, the microstructure can be divided into several regions of significance based on morphology: the columnar, the equiaxed, and the high burnup structure regions. Each region reflects a temperature regime that governs various microstructure evolution mechanisms and is characterized by a different defect population, composition, and physical properties. The thermal characterization reported here complements the extensive chemical and mechanical characterization already performed on SFR MOX samples for the development and validation of mechanistic fuel performance models.

2. Experimental Methods

2.1 Sample Information and Preparation

The MOX sample analyzed here was part of the Core Demonstration Experiment (CDE) conducted at the Fast Flux Test Facility (FFTF) in subassembly ACO-3 (*25*). Operation occurred between Aug. 17th, 1985, and March 13th, 1992, reaching a maximum of 1500 Effective Full Power Days (EFPD), and a peak FIMA (fissions per initial metal atom) of 23% at the axial center of the fuel rod (*26*). The peak fast

fluence achieved during operation for ACO-3 was 38.9×10^{22} n/cm^2 (E > 0.1 MeV), and a peak linear power of 39.6 kW/m. The burnup of the sample, estimated from analytical chemistry of the fission products, is 19% FIMA (*27*). The thermal analysis for this fuel rod reported by a previous study estimates the centerline temperature was maintained in the 1700-1900 °C range (*28*). The design parameters of the fuel rod are listed in Table 1. The theoretical density (%TD) is the ratio of the fuel density considering pores to the fully dense fuel. The smeared density is the cross-section fractional area of the fuel within the fuel rod.

Table 1. Design parameters of the sample fuel rod (*27*).

Design Parameters		
Cladding		HT-9 (>8% wt Cr steel)
	Outer radius (mm)	3.429
	Cladding thickness (mm)	0.559
Fuel		$(U, Pu)O_2$
	Outer radius (mm)	2.775
	Inner radius (mm)	0.737
	Gap width (mm)	0.095
	Smeared density (%TD)	80.0 ± 4.1
	Pellet density (%TD)	92.0
	Initial O to M	1.95 ± 0.03
	Plutonium (wt %)	29
	BOL/EOL Surface temperature (°C)	847/813
	EOL Centerline temperature (°C)	1736

The sample was cut into a 2-3 mm thick slice, ground to 1mm in thickness to reduce radioactivity, and finally polished to a 0.25 μm surface roughness finish using a diamond paste (*26*). The sample was further divided into a segment of about a quarter of a disk to further reduce radioactivity and protect the instruments and optics that are present in the TCM.

The measurement locations are indicated on an optical image of the fuel fragment shown in Figure 1. Post-irradiation examination of the fuel rod showed that the central void radius had grown to 0.850 mm after operation (*26*). The geometric center of the fuel disk segment was chosen as the origin used to calculate radial distances. Due to swelling of the central void and fuel pellet, beginning-of-life (BOL) relative radial distances may be slightly offset compared to end-of-life distances (*29*).

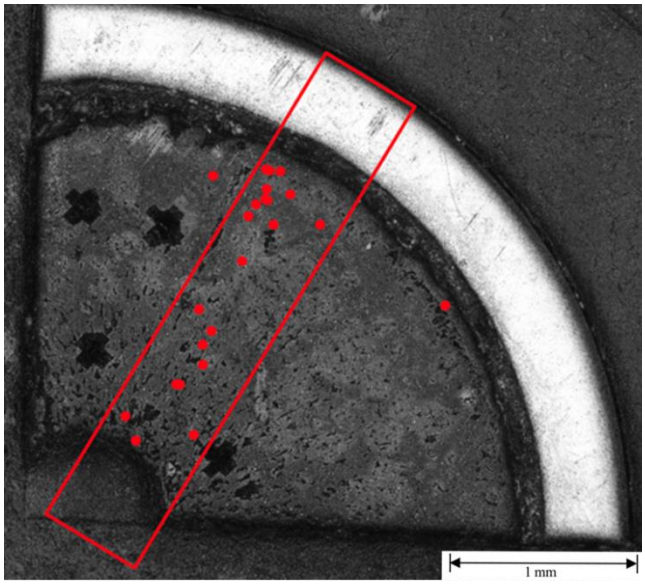

Figure 1. Optical image of a fuel segment used for thermal measurements. Locations of thermal diffusivity and thermal conductivity measurement are identified with red dots, the rectangle denotes the radial axis.

2.2 Thermal Conductivity Measurement

The Thermal Conductivity Microscope (TCM) is an instrument that uses a thermoreflectance technique to measure the localized thermal conductivity of materials (*16*, *30*). It consists of pump and probe lasers, emitting light at 660 nm and 532 nm wavelengths, respectively. A thin film of gold (59.6 nm) is deposited on the surface, which acts as a transducer layer for thermal measurement owing to its high thermoreflectance coefficient at 532 nm. Both beams are focused on the sample surface using a microscope objective (*17*). The pump's laser intensity is electronically modulated using a function generator and is used to heat the surface of the sample locally, resulting in a periodically oscillating temperature profile, casually referred to as a thermal wave. The probe laser is used to spatially measure the surface temperature by scanning across the pump laser location and directing the resulting temperature-induced reflection using a lock-in amplifier. At each measurement location, the phase lag between the pump modulation and probe reflection is recorded as a function of the two beams' separation distance. The beams are spatially displaced over tens of micrometers. This is repeated over a 1-100 kHz range of pump modulation frequencies. These phase profiles are fitted to the solution of a heat diffusion equation to extract the conductivity of the sample (*15*, *16*). This procedure generally requires a knowledge of specific heat. Nevertheless, an additional set of measurements can be performed to simultaneously measure conductivity and diffusivity (*16*).

3. Results

Measured thermal conductivity and diffusivity values as a function of radial position away from the fuel pin center are shown in Figure 2. For this study, we define three separate geometric regions of the fuel pellet: the central region, the mid-radial region, and the periphery region. In the central region, thermal conductivity gradually increases moving away from the center. In the periphery, a much larger variation of thermal conductivity is observed. In the mid-radial region, only a single measurement at 0.7 relative radius was obtained due to challenges in finding locations for performing a high-quality

measurement. Initial expectations for the decrease in conductivity near the periphery were confirmed by a drastic reduction in fuel conductivity likely owing to the high burnup structure formation (HBS). In addition to the localized variations of thermal conductivity that are measured, both variations of specific heat and density affect to the measured values of thermal diffusivity.

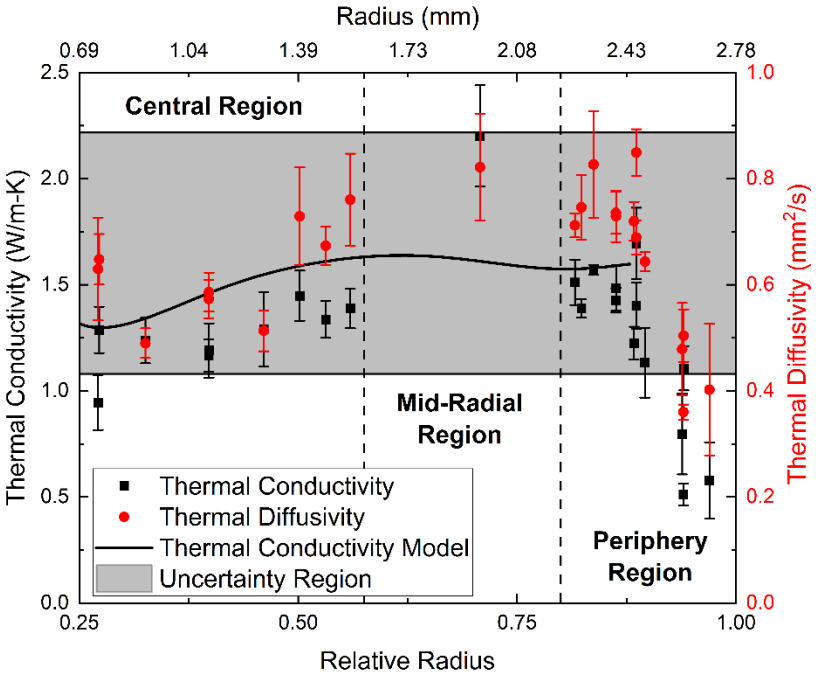

Figure 2. The radial profile of measured thermal conductivity to the prediction of the Lucuta-Inoue correlations for thermal conductivity using the assumption discussed in section 4. The shaded region captures the uncertainty bounded by 0-8 % porosity and stoichiometry between 1.9-2.0 at a uniform 19% FIMA. Because the Lucuta-Inoue model is not parameterized for HBS effects, the outer periphery region is not modeled.

4. Thermal Conductivity Radial Profile Modeling

To analyze our measured results, we utilize a physics-based, experimentally parameterized thermal conductivity model outlined by Lucuta *et. al* (*4*). While the original treatment is for UO_2 instead of MOX, we modify the unirradiated conductivity using Inoue's correlation, which was parameterized for MOX fuel between room temperature and 1850K (*31*, *32*). Recent efforts to improve the efficacy of MOX fuel performance models have been proposed, including expanding upon specific defect mechanisms considered in the Lucuta model (*33-35*). However, due to its widely accepted use, we chose to use the Lucuta-Inoue model. It has a form generally used in fuel performance codes considering pristine bulk thermal conductivity corrected by a set of multipliers accounting for in-pile and thermal degradation mechanisms such as (1) dissolved and (2) solid precipitate fission products, (3) radiation-induced point defects and defect clusters, and (4) porosity:

$$k_{irr}(r) = k_0 F_{dis} F_{prec} F_{rad} F_{por} \quad (1)$$

Inoue proposed the following equation to estimate the unirradiated fully dense, fresh MOX fuel thermal conductivity in units of W/mK is given (*31*):

$$k_0 = \frac{1}{0.06059 + 0.2754\sqrt{x} + 2.011 \times 10^{-4} T_{meas}} + \frac{4.715 \times 10^9}{T_{meas}^2}\ exp\left(-\frac{16361}{T_{meas}}\right) \quad (2)$$

where T is the fuel temperature in Kelvin and x is the deviation of oxygen stoichiometry from 2. Since the fuel is still radioactive, we use 50°C for measurement temperature. Although there is some uncertainty regarding the actual value, the effect on the model due to the deviation from this temperature is minimal. The deviation from non-stoichiometry (x) is taken as a constant, given in Table 1. The unirradiated conductivity is modified by the four pragmatic correlations (Eq. 1).

F_{dis} describes the effect of dissolved fission products in the matrix using the Klemens model for point defects which explicitly considers the physics of phonon scattering with defects (*5*, *36*). It recognizes that heat is carried by lattice vibrations of different wavelengths and the rate of scattering with defects is wavelength dependent. This term was parameterized based on fitting the scattering term to simulated high burnup UO_2 fuel (known as SIMFUEL), specifically fabricated for separate effects testing (*37*, *38*). SIMFUEL mimics the elemental composition of irradiated UO_2 fuel. In UO_2, F_{dis} captures the effect of soluble fission products in the matrix and plutonium build-up (*4*). These differences in capturing the effect of Pu have little impact as the impact of plutonium itself on thermal conductivity is minimal due to the slight mass mismatch between Pu and U atoms. The effect of its depletion and buildup are often neglected, but still present, particularly at concentrations higher than that seen in MOX fuel (*39*). The impact of soluble fission products is given as (*10*, *40*):

$$F_{dis}(T, \beta) = \left(\frac{1.09}{\beta^{3.265}} + \frac{0.0643}{\sqrt{\beta}}\sqrt{T_{meas}}\right)\arctan\left(\frac{1.09}{\beta^{3.265}} + \frac{0.0643}{\sqrt{\beta}}\sqrt{T_{meas}}\right)^{-1} \quad (3)$$

where β is the burnup in units of FIMA. It should be noted that the parameters in Eq. 3 are based on the fission product inventory of UO_2 under thermal neutron sources. For simplicity, we use Eq. 3 as is.

F_{prec} term describes thermal conductivity increase due to solid precipitate fission products in the matrix. Although the volume fractions of solid precipitates is expected to vary between reactor and fuel type, a similar increase in MOX, as in UO_2, conductivity has been observed (*41*). Since the mostly metallic precipitates have a higher thermal conductivity than that of the matrix fuel, their contribution to the effective thermal conductivity is positive (*4*, *5*), and their impacts are modeled using an effective medium approximation with a temperature dependent factor that accounts for their precipitation when fuel temperature exceeds a threshold (*42*, *43*):

$$F_{prec}(T, \beta) = 1 + \frac{0.019\beta}{(3 - 0.019\beta)\left(1 + \exp\left(\frac{-(T_{irr} - 1200)}{100}\right)\right)} \quad (4)$$

At the onset of irradiation, there is a loss of low-temperature conductivity due to rapid accumulation of radiation damage, defined by Lucuta as neutron, α- particle, and fission damage. F_{rad} describes these cumulative early-stage defects of radiation damage which have an impact only at low temperatures (*4*, *22*, *44*):

$$F_{rad} = 1 - \frac{0.2}{1 + exp\left(\frac{T_{irr} - 900}{80}\right)} \quad (5)$$

While the original formulation of F_{rad} was phenomenological (*4*), a recent study provides a mechanistic description for this parameter and suggests that F_{rad} is primarily caused by the accumulation of point defects whose concentration is significant only below stage II for the annealing of uranium sub-lattice defects (*11*).

Finally, the Loeb correlation accounts for porosity effects on thermal conductivity (F_{por}) and is given by:

$$F_{por} = 1 - \alpha\rho \qquad (6)$$

where α is taken as 2.5 for porosity fractions less than 10% *(45)*. Owing to the unique aspects of the TCM, Eq. 6 should only be used to capture the effect of pores smaller than 1 μm. Treatment of fission gas bubbles smaller than a few nm requires a different approach that recognizes that lattice vibrations of different wavelengths are impacted differently by nanoscale defects (*19, 46*).

Figure 3 shows an analysis of the effects of temperature on correction factors of the Lucuta model. This describes how the effects of precipitates, both soluble and insoluble, as well as irradiation damage influence the unirradiated thermal conductivity of the fuel. F_{pore} does not explicitly depend on temperature or burnup and is not included in Fig. 3.

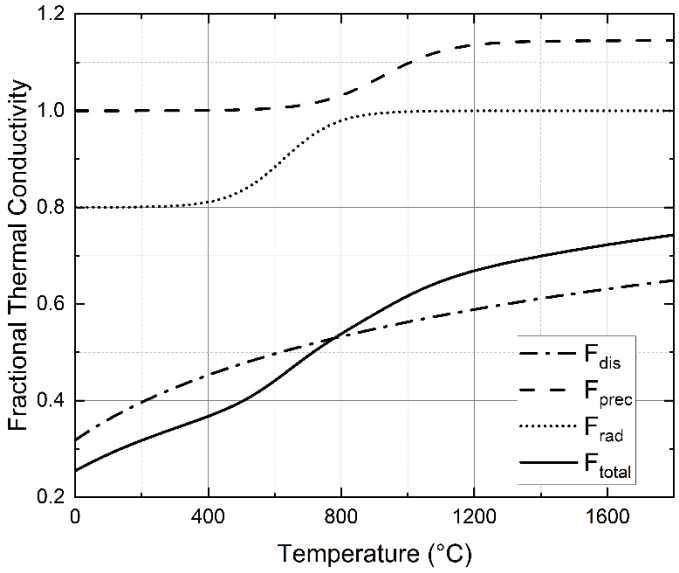

Figure 3. Temperature dependence of the thermal conductivity modifiers due to reactor operation ($T_{meas} = T_{irr}$) at 19% FIMA in the Lucuta model. F_{total} represents the cumulation of the first three modifiers listed in Eq. 3-5.

Applying the above model to current experimental results, we need to revisit the choice of temperatures in different expressions. The temperatures in the Lucuta model correspond to the temperature experienced by the fuel while in service, which can be referred to as in-pile temperature. However, our measurements are performed at ambient conditions close to room temperature (*11*). We recognize that in Eq. 2 and 3, T_{meas} corresponds to a temperature at which conductivity is measured,

while in Eq. 4 it is the highest temperature experienced by the fuel, which should correspond to in-pile temperature, or T_{irr}.

The discussion of temperature in Eq. 5 is complicated by the self-irradiation effect (*12, 14*). The build-up of short-lived Pu isotopes and other minor actinides (e.g., Am) contributes to the emission of alpha particles that create displacement damage in the form of point defects (47, 48). The purpose of Eq. 5 is to capture this kind of damage, though it was originally introduced to capture the effects taking place in-pile (4, 12). In the current analysis, we repurpose its utilization to capture the effect of self-irradiation, as both processes have been shown to have similar effects on thermal properties once defects concentrations have reached equilibrium concentration (49). Figure 4 compares the thermal conductivity of three cases corresponding to the in-pile, out-of-pile, and out-of-pile with self-irradiated conductivity profiles. These calculations are based on in-pile temperature calculated assuming a linear power rate of 30 kW/m.

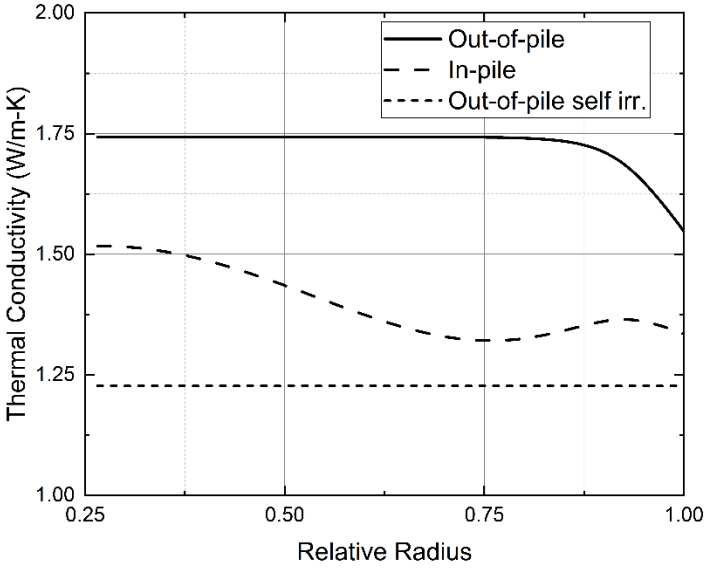

Figure 4. Different thermal conductivity profiles for the fuel sample with the as-designed porosity and stoichiometry, and a constant burnup function of 19% FIMA.

To enable direct comparison of experimental results to the Lucuta model, we need to make several additional assumptions related to microstructure. Detailed characterization of porosity, stoichiometry, and fission product precipitates is not available for this sample. Therefore, non-stoichiometry and porosity values are assumed to remain the same as the design parameters listed in Table 1. This assumption is justified when one considers the parametric analysis presented in Figure 3. One notices that dissolved fission products (Eq. 3) have the largest impact on thermal conductivity. Therefore, it is expected that the shape of the curve is largely governed by the burnup profile, especially in cases of very high burnup levels.

To demonstrate this point, we made a qualitative estimate of the local burn-up parameter across the radial profile of the fuel. We consider a sample taken from a different fuel assembly, located at a different

axial height (6.32% FIMA). The neodymium (Nd) concentration profile measured by electron probe micro-analyzer (EPMA) has been previously reported (*50*). From the radial concentration, the radial burnup profile was estimated. It is assumed that at higher burnup the radial profile is retained. The extrapolated profile of Nd is shown in Fig. 5. The function used to fit the data is a 5th-order polynomial which is scaled to 19% FIMA by a cumulative burnup ratio, while maintaining a equal radial integral burnup value.

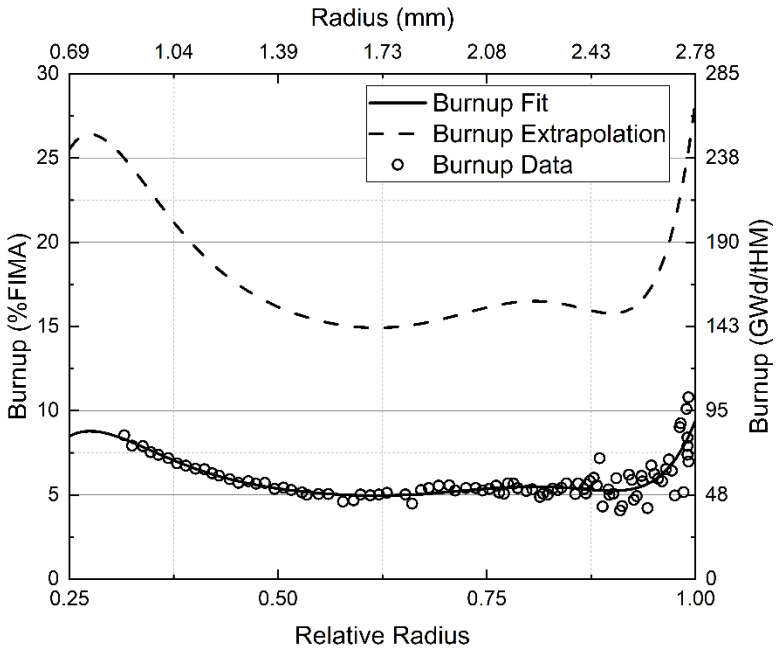

Figure 5. Dotted EPMA data of the measured burnup profile (6.32% FIMA) taken from Nd measurements along with straight line fit (50). The dashed line shows the extrapolation to 19% FIMA.

5. Discussion

The experimental results presented here complement previous measurements of a lower burnup (13.7% FIMA) SFR MOX fuel conductivity using TCM (*23*). The conductivity profiles presented in the current and previous studies exhibit similar radial shapes, but the magnitudes are notably different. Our results are consistent with the lower burnup (13.7% FIMA) sample which also exhibited a gradual increase as we moved from the central region towards the periphery region, reaching a maximum value at around 0.7 relative radius, and a notable reduction in the periphery. In contrast to the previous study, we perform further analysis that compares measurements to existing correlations.

The Lucuta-Inoue model was chosen for this comparison due to its simple and convenient approach to capturing various microstructural features. In contrast, Duriez-NFI and the Amaya models developed for high burn-up MOX fuel, only go as high as 7%-8% FIMA (*40, 50, 51*). One limitation of the Lucuta model is that its dissolved fission product correction is based on the inventory for light water reactor UO_2 fuel. Several other attempts to modify Eq. 3 specific to MOX under fast neutron conditions have been made, however, they provide expressions which require knowledge of the inventory of fission products (*34, 52*). Parameters needed to perform an accurate estimation of the inventory of fission products in our sample are not available. Therefore, the best available option is to use the correlation provide by the Lucuta model.

Figure 2 compares the experimental results and prediction of the Lucuta-Inoue model focusing on the adequacy of this model to predict radially resolved thermal conductivity in MOX fuel. Experimental data falls within the uncertainty range predicted by the model. For a more accurate comparison, further work is needed to determine how pores of different sizes impact thermal conductivity measurements by TCM. It should be also recognized that Eq. 6 is applicable for large-scale porosity and treatment of nanoscale fission gas bubbles and dislocations requires a modified approach that is not currently captured by existing correlations (*19, 46, 54, 55*).

We focus on three distinct regions identified in Figure 2, namely the central, mid, and periphery regions. Migration of pores from across the fuel to the central region causes the growth of the central void. The central region immediately outside of the central void is characterized by columnar grains and lenticular pores resulting from the vaporization-condensation mechanism (mass transport along the temperature gradient) within the fuel at temperatures above 1800°C (*26, 56*). The mid-radial region is typically represented by equiaxed grains and a high density of small pores likely resulting from an accumulation of fission gas atoms. The periphery undergoes more significant restructuring and exhibits the high burn-up structure and formation of the "*Joint Oxyde-Gaine*" (JOG) phase (*27, 57, 58*).

5.1 Central Region

The Lucuta-Inoue model shows good agreement at the central columnar region, despite not explicitly considering the restructuring and vaporization caused by the high temperatures. This may not be surprising considering that in this temperature region, dissolved fission products are the primary contributors to the reduction of thermal conductivity (Figure 4). However, we cannot rule out a cancelation of error. Our current analysis does not account for oxygen stoichiometry and Pu redistribution due to the Soret effect (*6, 59*). Reactor operation causes large non-stoichiometry variation across the pellet radius in hypo-stoichiometric MOX (*6, 59*). The Soret effect causes the plutonium from the mid-radial region to diffuse to the central regions due to the high temperature and temperature gradient, whereas oxygen non-stoichiometry is governed by excess oxygen resulting from the consumption of fissile atoms. Both mechanisms would decrease the thermal conductivity. Alternatively, damage accumulation during storage might not have been properly accounted for using the low temperature correlation in Eq. 5. The maximum estimated temperature this fuel reached should induce whole or partial columnar grain formation (*28*).

5.2 Mid-Radial Region

The maximum thermal conductivity found at 0.7 relative radius is poorly captured by the model. However, considering the limited data in the mid-radial region, owing to the difficulty in performing measurements in this region, conclusions should be taken lightly. As stated before the same trend in data was observed in another similar experiment, where a maximum in the conductivity profile was reached near the center of the fuel pellet (*23*). That same profile is likely observed in this sample as it was in the 13.7% FIMA sample.

5.3 Periphery

The periphery region of the sample contains the HBS and JOG sections of the fuel. In this region, at burnup exceeding 7-8% FIMA, the HBS, and the JOG often form (*27, 57*). The HBS forms due to several region-specific thermal and microstructural conditions (*60*); 1) the lower temperature in this region causes defect accumulation due to the low defect mobility which inhibits the annealing of defects (*11, 47, 61*); 2)

the polygonization of dislocations /granular subdivision (*3*, *62*, *63*); 3) the recrystallization of defect-free nano-metric grains to reduce the Gibbs free energy of the highly strained lattice (*62*, *64*).

The periphery region is not hot enough to cause grain growth but exhibits nano-metric pores filled with Xe–fission gas due to a smaller intragranular gas inventory in nanometric grains (*65*). The fission gas-filled intergranular bubbles/pores in the HBS represent an insulating secondary phase which further decreases the thermal conductivity in the periphery region. The recrystallization of the grains (leading to defect-free grains initially) in this region could be expected to increase thermal conductivity in the initial stages of the HBS. Considering that the Lucuta-Inoue model as used in this study was not parameterized to consider the grain size, the measured values are reasonably lower than the calculated values by the model. The porosity (fission gas bubbles before FGR) and nano-metric grains, which are microstructural characteristics of the HBS, could be expected to degrade the effective thermal conductivity of the fuel down to 1 W/mK (*60*).

6. Conclusion

The thermal conductivity of irradiated SFR MOX fuel has been measured using a laser-based thermal conductivity microscope to better understand thermal conductivity profiles in high burnup fuel. Existing thermal conductivity correlations, namely the Inoue model of fresh MOX fuel combined with pragmatic modifiers by Lucuta were used to estimate the thermal conductivity across the radial direction. Both models are physics-based and suitable for further refinement based on microstructure information. We find that the Lucuta-Inoue model provides a reasonable estimate in the central region. It provides an inadequate estimate in the periphery region as the model does not capture the effects associated with the formation of the high burnup structure. Further studies that better capture plutonium redistribution, oxygen stoichiometry, and microstructure in the periphery region across different burnup levels are needed to improve the model.

Acknowledgements

This work was supported through the INL Laboratory Directed Research& Development (LDRD) Program under DOE Idaho Operations Office Contract DE-AC07-05ID14517. This work was also supported by the U.S. Department of Energy, Office of Nuclear Energy under DOE Idaho Operations Office Contract DE-AC07- 05ID14517 as part of a Nuclear Science User Facilities experiment.

References

1. C. T. Walker *et al.*, On the thermal conductivity of UO2 nuclear fuel at a high burn-up of around 100MWd/kgHM. *Journal of Nuclear Materials* **350**, 19-39 (2006).
2. D. Olander, Nuclear fuels – Present and future. *Journal of Nuclear Materials* **389**, 1-22 (2009).
3. X.-M. Bai, M. R. Tonks, Y. Zhang, J. D. Hales, Multiscale modeling of thermal conductivity of high burnup structures in UO2 fuels. *Journal of Nuclear Materials* **470**, 208-215 (2016).
4. P. G. Lucuta, H. Matzke, I. J. Hastings, A pragmatic approach to modelling thermal conductivity of irradiated UO2 fuel: Review and recommendations. *Journal of Nuclear Materials* **232**, 166-180 (1996).
5. D. H. Hurley *et al.*, Thermal Energy Transport in Oxide Nuclear Fuel. *Chemical Reviews* **122**, 3711-3762 (2022).
6. K. Lassmann, TRANSURANUS: a fuel rod analysis code ready for use. *Journal of Nuclear Materials* **188**, 295-302 (1992).

7. V. Marelle *et al.*, "New developments in ALCYONE 2.0 fuel performance code," (American Nuclear Society, United States, 2016).
8. R. L. Williamson *et al.*, BISON: A Flexible Code for Advanced Simulation of the Performance of Multiple Nuclear Fuel Forms. *Nuclear Technology* **207**, 954-980 (2021).
9. M. Lainet, B. Michel, J.-C. Dumas, M. Pelletier, I. Ramière, GERMINAL, a fuel performance code of the PLEIADES platform to simulate the in-pile behaviour of mixed oxide fuel pins for sodium-cooled fast reactors. *Journal of Nuclear Materials* **516**, 30-53 (2019).
10. J. J. Carbajo, G. L. Yoder, S. G. Popov, V. K. Ivanov, A review of the thermophysical properties of MOX and UO2 fuels. *Journal of Nuclear Materials* **299**, 181-198 (2001).
11. J. Ferrigno, S. Adnan, M. Khafizov, Influence of point defect accumulation on in-pile thermal conductivity degradation: Fuel rod defect distribution and deviation between in-pile and post irradiation thermal conductivity. *Journal of Nuclear Materials*, 154108 (2022).
12. C. Ronchi, M. Sheindlin, D. Staicu, M. Kinoshita, Effect of burn-up on the thermal conductivity of uranium dioxide up to 100.000 MWdt−1. *Journal of Nuclear Materials* **327**, 58-76 (2004).
13. D. Staicu *et al.*, Thermal conductivity of homogeneous and heterogeneous MOX fuel with up to 44 MWd/kgHM burn-up. *Journal of Nuclear Materials* **412**, 129-137 (2011).
14. D. Staicu *et al.*, Effect of burn-up on the thermal conductivity of uranium–gadolinium dioxide up to 100GWd/tHM. *Journal of Nuclear Materials* **453**, 259-268 (2014).
15. Z. L. Hua *et al.*, Spatially localized measurement of thermal conductivity using a hybrid photothermal technique. *Journal of Applied Physics* **111**, 103505 (2012).
16. D. Hurley, R. Schley, M. Khafizov, B. Wendt, Local measurement of thermal conductivity and diffusivity. *Review of Scientific Instruments* **86**, (2015).
17. M. Khafizov *et al.*, Investigation of thermal transport in composites and ion beam irradiated materials for nuclear energy applications. *Journal of Materials Research* **32**, 204-216 (2017).
18. J. Pakarinen *et al.*, Microstructure changes and thermal conductivity reduction in UO2 following 3.9 MeV He2+ ion irradiation. *Journal of Nuclear Materials* **454**, 283-289 (2014).
19. M. Khafizov, J. Pakarinen, L. He, D. H. Hurley, Impact of irradiation induced dislocation loops on thermal conductivity in ceramics. *Journal of the American Ceramic Society* **102**, 7533-7542 (2019).
20. C. A. Dennett *et al.*, An integrated experimental and computational investigation of defect and microstructural effects on thermal transport in thorium dioxide. *Acta Materialia* **213**, 116934 (2021).
21. A. Abdullaev *et al.*, Depth-resolved thermal conductivity and damage in swift heavy ion irradiated metal oxides. *Journal of Nuclear Materials* **561**, (2022).
22. A. J. Terricabras *et al.*, Thermal conductivity evaluation of ion irradiated Si3N4 and ZrN ceramics using spatial domain thermoreflectance. *Journal of Applied Physics* **132**, 075105 (2022).
23. C. McKinney *et al.*, Three-dimensional microstructural characterization of FBR MOX fuel and the contribution of microstructural features to the thermal conductivity of the fuel. *Journal of Nuclear Materials* **572**, 154073 (2022).
24. T. R. Pavlov *et al.*, Understanding the local thermal conductivity evolution of neutron irradiated U3Si2 dispersion fuel via state-of-the-art thermo-reflectance measurements. *Journal of Nuclear Materials* **557**, 153280 (2021).
25. J. L. Ethridge, R. B. Baker, R. D. Leggett, A. L. Pitner, A. E. Waltar, "Fast Flux Test Facility core system," (United States, 1990).
26. M. C. Teague, Ph.D., Colorado School of Mines, Ann Arbor (2013).
27. F. Cappia *et al.*, Electron microscopy characterization of fast reactor MOX Joint Oxyde-Gaine (JOG). *Journal of Nuclear Materials* **531**, 151964 (2020).

28. M. Teague, M. Tonks, S. Novascone, S. Hayes, Microstructural modeling of thermal conductivity of high burn-up mixed oxide fuel. *Journal of Nuclear Materials* **444**, 161-169 (2014).
29. R. J. Parrish, F. Cappia, A. Aitkaliyeva, Comparison of the radial effects of burnup on fast reactor MOX fuel microstructure and solid fission products. *Journal of Nuclear Materials* **531**, 152003 (2020).
30. C. A. Adkins *et al.*, "Demonstrate Thermal Property Measurement on Irradiated Fuel in IMCL," (United States, 2019).
31. M. Inoue, Thermal conductivity of uranium–plutonium oxide fuel for fast reactors. *Journal of Nuclear Materials* **282**, 186-195 (2000).
32. M. Inoue *et al.*, Fuel-to-cladding gap evolution and its impact on thermal performance of high burnup fast reactor type uranium–plutonium oxide fuel pins. *Journal of Nuclear Materials* **326**, 59-73 (2004).
33. A. Magni *et al.*, Modelling and assessment of thermal conductivity and melting behaviour of MOX fuel for fast reactor applications. *Journal of Nuclear Materials* **541**, 152410 (2020).
34. P. Bonev *et al.*, New recommendation for the thermal conductivity of irradiated (U, Pu)O2 fuels under fast reactor conditions. Comparison with recent experimental data. *Journal of Nuclear Materials* **577**, 154326 (2023).
35. A. Bouloré *et al.*, Modelling of UO2 thermal conductivity: Improvement of the irradiation defects contribution and uncertainty quantification. *Nuclear Engineering and Design* **407**, 112304 (2023).
36. P. G. Klemens, Thermal conductivity and lattice vibration modes. *Solid State Physics-Advances in Research and Applications* **7**, 1-98 (1958).
37. P. G. Klemens, Thermal Resistance due to Point Defects at High Temperatures. *Physical Review* **119**, 507-509 (1960).
38. P. G. Lucuta, H. Matzke, R. A. Verrall, Modelling of UO2-based SIMFUEL thermal conductivity The effect of the burnup. *Journal of Nuclear Materials* **217**, 279-286 (1994).
39. C. Cozzo, D. Staicu, J. Somers, A. Fernandez, R. J. M. Konings, Thermal diffusivity and conductivity of thorium–plutonium mixed oxides. *Journal of Nuclear Materials* **416**, 135-141 (2011).
40. M. Amaya, J. Nakamura, F. Nagase, T. Fuketa, Thermal conductivity evaluation of high burnup mixed-oxide (MOX) fuel pellet. *Journal of Nuclear Materials* **414**, 303-308 (2011).
41. A. International Atomic Energy, "Water reactor fuel element computer modelling in steady state, transient and accident conditions," (International Atomic Energy Agency (IAEA), 1989).
42. P. G. Klemens, Anharmonic Attenuation of Localized Lattice Vibrations. *Physical Review* **122**, 443-445 (1961).
43. P. G. Klemens, Thermal conductivity of inhomogeneous materials. *International Journal of Thermophysics* **10**, 1213-1219 (1989).
44. V. S. Chauhan *et al.*, Comprehensive characterization of irradiation induced defects in ceria: Impact of point defects on vibrational and optical properties. *Journal of Applied Physics* **132**, 085105 (2022).
45. A. Shrivastava, R. Shukla, P. Chaudhuri, Effect of porosity on thermal conductivity of Li2TiO3 ceramic compact. *Fusion Engineering and Design* **166**, 112318 (2021).
46. S. Nichenko, D. Staicu, Thermal conductivity of porous UO2: Molecular Dynamics study. *Journal of Nuclear Materials* **454**, 315-322 (2014).
47. W. J. Weber, Thermal recovery of lattice defects in alpha-irradiated UO2 crystals. *Journal of Nuclear Materials* **114**, 213-221 (1983).
48. S. J. Zinkle, in *Comprehensive Nuclear Materials,* R. J. M. Konings, Ed. (Elsevier, Oxford, 2012), pp. 65-98.

49. D. Staicu *et al.*, Impact of auto-irradiation on the thermophysical properties of oxide nuclear reactor fuels. *Journal of Nuclear Materials* **397**, 8-18 (2010).
50. F. Cappia, J. Harp, "Microstructural and chemical characterization of medium burnup fast reactor MOX using electron microscopy," (United States, 2021).
51. C. Duriez, J.-P. Alessandri, T. Gervais, Y. Philipponneau, Thermal conductivity of hypostoichiometric low Pu content (U,Pu)O2−x mixed oxide. *Journal of Nuclear Materials* **277**, 143-158 (2000).
52. D. D. Lanning, C. E. Beyer, K. J. Geelhood. (Pacific Northwest National Laboratory, 2005), vol. 4.
53. Y. Horii *et al.*, Thermal conductivity measurement of uranium–plutonium mixed oxide doped with Nd/Sm as simulated fission products. *Journal of Nuclear Materials* **588**, 154799 (2024).
54. W. M. Chen, M. W. D. Cooper, Z. Q. Xiao, D. A. Andersson, X. M. Bai, Effect of Xe bubble size and pressure on the thermal conductivity of UO2-A molecular dynamics study. *Journal of Materials Research* **34**, 2295-2305 (2019).
55. M. M. Jin, C. A. Dennett, D. H. Hurley, M. Khafizov, Impact of small defects and dislocation loops on phonon scattering and thermal transport in ThO2. *Journal of Nuclear Materials* **566**, (2022).
56. M. J. Welland, in *Comprehensive Nuclear Materials (Second Edition),* R. J. M. Konings, R. E. Stoller, Eds. (Elsevier, Oxford, 2020), pp. 200-247.
57. M. Teague, B. Gorman, J. King, D. Porter, S. Hayes, Microstructural characterization of high burn-up mixed oxide fast reactor fuel. *Journal of Nuclear Materials* **441**, 267-273 (2013).
58. J. Noirot, L. Desgranges, J. Lamontagne, Detailed characterisations of high burn-up structures in oxide fuels. *Journal of Nuclear Materials* **372**, 318-339 (2008).
59. K. Lassmann, The oxired model for redistribution of oxygen in nonstoichiometric uranium-plutonium oxides. *Journal of Nuclear Materials* **150**, 10-16 (1987).
60. M. Khafizov *et al.*, Thermal Conductivity in Nanocrystalline Ceria Thin Films. *Journal of the American Ceramic Society* **97**, 562-569 (2014).
61. S. J. Zinkle, in *Comprehensive Nuclear Materials*. (Elsevier, Oxford, 2012), pp. 65-98.
62. B.-H. Lee, Y.-H. Koo, D.-S. Sohn, Rim Characteristics and Their Effects on the Thermal Conductivity in High Burnup UO2 Fuel. *Journal of Nuclear Science and Technology* **38**, 45-52 (2001).
63. H. Kämpf, G. Karsten, Effects of Different Types of Void Volumes on the Radial Temperature Distribution of Fuel Pins. *Nuclear Applications and Technology* **9**, 288-300 (1970).
64. H. Xiao, C. Long, H. Chen, The formation mechanisms of high burnup structure in UO2 fuel. *Journal of Nuclear Materials* **556**, 153151 (2021).
65. J. Noirot, L. Desgranges, J. Lamontagne, Detailed characterisations of high burn-up structures in oxide fuels. (2008).